
MiME: Multilevel Medical Embedding of Electronic Health Records for Predictive Healthcare

Edward Choi*
Google Brain
edwardchoi@google.com

Cao Xiao
IBM Research
cxiao@us.ibm.com

Walter F. Stewart†
HINT Consultants
wfs502000@yahoo.com

Jimeng Sun
Georgia Institute of Technology
jsun@cc.gatech.edu

Abstract

Deep learning models exhibit state-of-the-art performance for many predictive healthcare tasks using electronic health records (EHR) data, but these models typically require training data volume that exceeds the capacity of most healthcare systems. External resources such as medical ontologies are used to bridge the data volume constraint, but this approach is often not directly applicable or useful because of inconsistencies with terminology. To solve the data insufficiency challenge, we leverage the inherent multilevel structure of EHR data and, in particular, the encoded relationships among medical codes. We propose Multilevel Medical Embedding (MiME) which learns the multilevel embedding of EHR data while jointly performing auxiliary prediction tasks that rely on this inherent EHR structure without the need for external labels. We conducted two prediction tasks, *heart failure prediction* and *sequential disease prediction*, where MiME outperformed baseline methods in diverse evaluation settings. In particular, MiME consistently outperformed all baselines when predicting heart failure on datasets of different volumes, especially demonstrating the greatest performance improvement (15% relative gain in PR-AUC over the best baseline) on the smallest dataset, demonstrating its ability to effectively model the multilevel structure of EHR data.

1 Introduction

The rapid growth of electronic health record (EHR) data has motivated use of deep learning models and demonstrated state-of-the-art performance in diagnostics [26, 13, 12, 27], disease detection [14, 10, 17], risk prediction [20, 32], and patient subtyping [3, 6]. However, training optimal deep learning models typically requires a large volume (*i.e.* number of patient records and features per record). Most health systems do not have the data volume required to optimize performance of these models, especially for less common services (*e.g.* intensive care units (ICU)) or rare conditions.

External resources, particularly medical ontologies have been used to address data volume insufficiencies [12, 31, 7]. For example [12], latent embedding of a clinical code (*e.g.* diagnosis code) can be learned as a convex combination of the embeddings of the code itself and its ancestors on the ontology graph. However, medical ontologies are often not available or not directly applicable due to the nonstandard, or idiosyncratic use of terminology and complex terminology mapping from one health system’s EHR to another. For example, many clinics still use their own in-house terminologies

*Work done at Georgia Institute of Technology.

†Work done at Sutter Health.

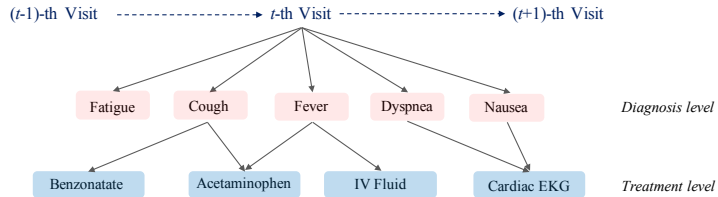


Figure 1: Symbolic representation of a single visit of a patient. Red denotes diagnosis codes, and blue denotes medication/procedure codes. A visit encompasses a set of codes, as well as a hierarchical structure and heterogeneous relations among these codes. For example, while both *Acetaminophen* and *IV fluid* form an explicit relationship with *Fever*, they also are correlated with each other as descendants of *Fever*.

for medications and lab tests, which do not conform with the standard medical ontologies such as Anatomical Therapeutic Chemical (ATC) Classification system and Logical Observation Identifiers Names and Codes (LOINC).

As an alternative, we explored how the inherent multilevel structure of EHR data could be leveraged to improve learning efficiency. The hierarchical structure of EHR data begins with the patient, followed by visits, then diagnosis codes within visits, which are then linked to treatment orders (e.g. medications, procedures). This hierarchical structure reveals influential multilevel relationships, especially between diagnosis codes and treatment codes. For example, a diagnosis *fever* can lead to associated treatments such as *acetaminophen* (medication) and *IV fluid* (procedure). We examine whether this multilevel structure could be leveraged to obtain a robust model under small data volume. To the best of our knowledge, none of the existing works leverage this multilevel structure in EHR. Rather, they flatten EHR data as a set of independent codes [18, 38, 11, 12, 14, 10, 13, 27, 2], which ignores hierarchical relationships among medical codes within visits.

We propose **Multilevel Medical Embedding** (MiME) to simultaneously transform the inherent multilevel structure of EHR data into multilevel embeddings, while jointly performing auxiliary prediction tasks that reflect this inherent structure without the need for external labels. Modeling the inherent structure among medical codes enables us to accurately capture the distinguishing patterns of different patient states. The auxiliary tasks inject the hierarchical knowledge of EHR data into the embedding process such that the main task can borrow prediction power from related auxiliary tasks. We conducted two prediction tasks, *heart failure prediction* and *sequential disease prediction*, where MiME outperformed baseline methods in diverse evaluation settings. In particular, for heart failure prediction on datasets of different volumes, MiME consistently outperformed all baseline models. Especially, MiME showed the greatest performance improvement (15% relative gain in PR-AUC over the best baseline) for the smallest dataset, demonstrating its ability to effectively model the multilevel structure of EHR data.

2 Method

EHR data can be represented by a common hierarchy that begins with individual patient records, where each patient record consists of a sequence of visits. In a typical visit, a physician gives a diagnosis to a patient and then order medications or procedures based on the diagnosis. This process generates a set of treatment (medication and procedure) codes and a relationship among diagnosis and treatment codes (see Figure 1). MiME is designed to explicitly capture the relationship between the diagnosis codes and the treatment codes within visits.

2.1 Notations of MiME

Assume a patient has a sequence of visits $\mathcal{V}^{(1)}, \dots, \mathcal{V}^{(t)}$ over time, where each visit $\mathcal{V}^{(t)}$ contains a varying number of diagnosis (Dx) objects $\mathcal{O}_1^{(t)}, \dots, \mathcal{O}_{|\mathcal{V}^{(t)}|}^{(t)}$. Each $\mathcal{O}_i^{(t)}$ consists of a single Dx code $d_i^{(t)} \in \mathcal{A}$ and a set of associated treatments (medications or procedures) $\mathcal{M}_i^{(t)}$. Similarly, each $\mathcal{M}_i^{(t)}$ consists of varying number of treatment codes $m_{i,1}^{(t)}, \dots, m_{i,|\mathcal{M}_i^{(t)}|}^{(t)} \in \mathcal{B}$. To reduce clutter, we omit

Table 1: Notations for MiME. Note that the dimension size z is used in many places due to the use of skip-connections, which will be described in section 2.2.

Notation	Definition
\mathcal{A}	Set of unique diagnosis codes
\mathcal{B}	Set of unique treatment codes (medications and procedures)
\mathbf{h}	A vector representation of a patient
$\mathcal{V}^{(t)}$	A patient’s t -th visit, which contains diagnosis objects $\mathcal{O}_1^{(t)}, \dots, \mathcal{O}_{ \mathcal{V}^{(t)} }^{(t)}$
$\mathbf{v}^{(t)} \in \mathbb{R}^z$	A vector representation of $\mathcal{V}^{(t)}$
$\mathcal{O}_i^{(t)}$	i -th diagnosis object of t -th visit consisting of Dx code $d_i^{(t)}$ and treatment codes $\mathcal{M}_i^{(t)}$
$\mathbf{o}_i^{(t)} \in \mathbb{R}^z$	A vector representation of $\mathcal{O}_i^{(t)}$
$p(d_i^{(t)} \mathbf{o}_i^{(t)}), p(m_{i,j}^{(t)} \mathbf{o}_i^{(t)})$	Auxiliary predictions, respectively for a Dx code and a treatment code based on $\mathbf{o}_i^{(t)}$
$d_i^{(t)} \in \mathcal{A}$	Dx code of diagnosis object $\mathcal{O}_i^{(t)}$
$\mathcal{M}_i^{(t)}$	a set of treatment codes associated with i -th Dx code $d_i^{(t)}$ in visit t
$m_{i,j}^{(t)} \in \mathcal{B}$	j -th treatment code of $\mathcal{M}_i^{(t)}$
$g(d_i^{(t)}, m_{i,j}^{(t)})$	A function that captures the interaction between $d_i^{(t)}$ and $m_{i,j}^{(t)}$
$f(d_i^{(t)}, \mathcal{M}_i^{(t)})$	A function that computes embedding of diagnosis object $\mathcal{O}_i^{(t)}$
$r(\cdot) \in \mathbb{R}^z$	A helper notation for extracting $d_i^{(t)}$ or $m_{i,j}^{(t)}$ ’s embedding vector

the superscript (t) indicating t -th visit, when we are discussing a single visit. Table 1 summarizes notations we will use throughout the paper.

In Figure 1, there are five Dx codes, hence five Dx objects $\mathcal{O}_1^{(t)}, \dots, \mathcal{O}_5^{(t)}$. More specifically, the first Dx object \mathcal{O}_1 has $d_1^{(t)} = \textit{Fatigue}$ as the Dx code, but no treatment codes. \mathcal{O}_2 , on the other hand, has Dx code $d_2^{(t)} = \textit{Cough}$ and two associated treatment codes $m_{2,1}^{(t)} = \textit{Benzonatate}$ and $m_{2,2}^{(t)} = \textit{Acetaminophen}$. In this case, we can use $g(d_2^{(t)}, m_{2,1}^{(t)})$ to capture the interaction between Dx code *Cough* and treatment code *Benzonatate*, which will be fed to $f(d_2^{(t)}, \mathcal{M}_2^{(t)})$ to obtain the vector representation of Dx object $\mathbf{o}_2^{(t)}$. Using the five Dx object embeddings $\mathbf{o}_1^{(t)}, \dots, \mathbf{o}_5^{(t)}$, we can obtain a visit embedding $\mathbf{v}^{(t)}$. In addition, some treatment codes (e.g. *Acetaminophen*) can be shared by two or more Dx codes (e.g. *Cough, Fever*), if the doctor ordered a single medication for more than one diagnosis. Then each Dx object will have its own copy of the treatment code attached to it, in this case denoted, $m_{2,2}^{(t)}$ and $m_{3,1}^{(t)}$, respectively.

2.2 Description of MiME

Multilevel Embedding As discussed earlier, previous approaches often flatten a single visit such that Dx codes and treatment codes are packed together so that a single visit $\mathcal{V}^{(t)}$ can be expressed as a binary vector $\mathbf{x}^{(t)} \in \{0, 1\}^{|\mathcal{A}|+|\mathcal{B}|}$ where each dimension corresponds to a specific Dx and treatment code. Then a patient’s visit sequence is encoded as:

$$\begin{aligned} \mathbf{v}^{(t)} &= \sigma(\mathbf{W}_x \mathbf{x}^{(t)} + \mathbf{b}_x) \\ \mathbf{h} &= h(\mathbf{v}^{(1)}, \mathbf{v}^{(2)}, \dots, \mathbf{v}^{(t)}) \end{aligned}$$

where \mathbf{W}_x is the embedding matrix that converts the binary vector \mathbf{x} to a lower-dimensional visit representation³, σ a non-linear activation function such as sigmoid or rectified linear unit (ReLU), $h(\cdot)$ a function that maps a sequence of visit representations $\mathbf{v}^{(0)}, \dots, \mathbf{v}^{(t)}$ to a patient representation \mathbf{h} . In contrast, MiME effectively derives a visit representation $\mathbf{v}^{(t)}$, than can be plugged into any $h(\cdot)$ for the downstream prediction task. $h(\cdot)$ can simply be an RNN or a combination of RNNs and CNN and attention mechanisms [1].

MiME explicitly captures the hierarchy between Dx codes and treatment codes depicted in Figure 1. Figure 2 illustrates how MiME builds the representation of \mathcal{V} (omitting the superscript (t)) in a bottom-up fashion via multilevel embedding. In a single Dx object \mathcal{O}_i , a Dx code d_i and its associated treatment codes \mathcal{M}_i are used to obtain a vector representation of \mathcal{O}_i , \mathbf{o}_i . Then multiple Dx object embeddings $\mathbf{o}_0, \dots, \mathbf{o}_{|\mathcal{V}|}$ in a single visit are used to obtain a visit embedding \mathbf{v} , which in turn forms

³We omit bias variables throughout the paper to reduce clutter.

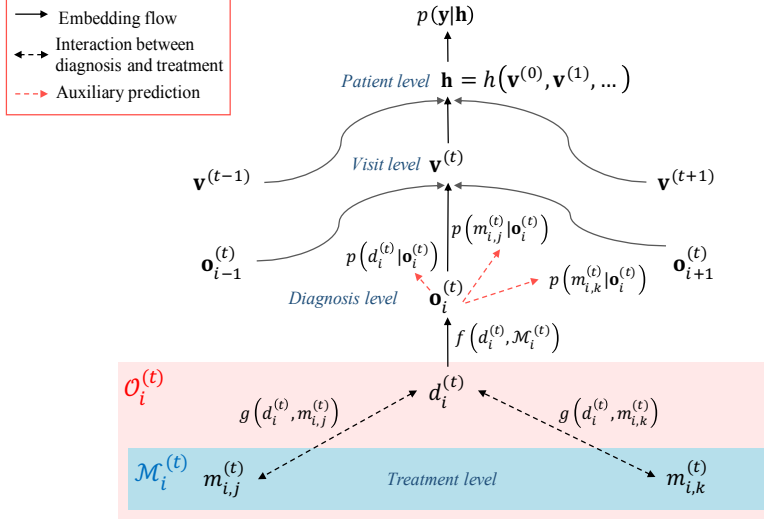


Figure 2: Prediction model using MiME. Codes are embedded into multiple levels: diagnosis-level, visit-level, and patient-level. Final prediction $p(y|h)$ is based on the patient representation \mathbf{h} , which is derived from visit representations $\mathbf{v}^{(0)}, \mathbf{v}^{(1)}, \dots$, where each $\mathbf{v}^{(t)}$ is generated using MiME framework. As shown in the *Treatment level*, MiME explicitly captures the interactions between a diagnosis code and the associated treatment codes. MiME also uses those codes as auxiliary prediction targets to improve generalizability when large training data are not available.

a patient embedding \mathbf{h} with other visit embeddings. The formulation of MiME is as follows:

$$\mathbf{v} = \sigma \left(\mathbf{W}_v \left(\underbrace{\sum_i^{|\mathcal{V}|} f(d_i, \mathcal{M}_i)}_{\text{F: used for skip-connection}} \right) \right) + F \quad (1)$$

$$f(d_i, \mathcal{M}_i) = \mathbf{o}_i = \sigma \left(\mathbf{W}_o \left(\underbrace{r(d_i) + \sum_j^{|\mathcal{M}_i|} g(d_i, m_{i,j})}_{\text{G: used for skip-connection}} \right) \right) + G \quad (2)$$

$$g(d_i, m_{i,j}) = \sigma(\mathbf{W}_m r(d_i)) \odot r(m_{i,j}) \quad (3)$$

where Eq. (1), Eq. (2) and Eq. (3) describe MiME in a top-down fashion, respectively corresponding to *Visit level*, *Diagnosis level* and *Treatment level* in Figure 2.

In Eq. (1), a visit embedding \mathbf{v} is obtained by summing Dx object embeddings $\mathbf{o}_1, \dots, \mathbf{o}_{|\mathcal{V}|}$, which are then transformed with $\mathbf{W}_v \in \mathbb{R}^{z \times z}$. σ is a non-linear activation function such as sigmoid or rectified linear unit (ReLU). In Eq. (2), \mathbf{o}_i is obtained by summing $r(d_i) \in \mathbb{R}^z$, the vector representation of the Dx code d_i , and the effect of the interactions between d_i and its associated treatments \mathcal{M}_i , which are then transformed with $\mathbf{W}_o \in \mathbb{R}^{z \times z}$. The interactions captured by $g(d_i, m_{i,j})$ are added to the $r(d_i)$, which can be interpreted as adjusting the diagnosis representation according to its associated treatments (medications and procedures). Note that in both Eq. (1) and Eq. (2), F and G are used to denote skip-connections [23].

In Eq. (3), the interaction between a Dx code embedding $r(d_i)$ and a treatment code embedding $r(m_{i,j})$ is captured by element-wise multiplication \odot . Weight matrix $\mathbf{W}_m \in \mathbb{R}^{z \times z}$ sends the Dx code embedding $r(d_i)$ into another latent space, where the interaction between d_i and the corresponding $m_{i,j}$ can be effectively captured. The formulation of Eq. (3) was inspired by recent developments in bilinear pooling technique [37, 21, 19, 24], which we discuss in more detail in Appendix A. With Eq. (3) in mind, G in Eq. (2) can also be interpreted as $r(d_i)$ being skip-connected to the sum of interactions $g(d_i, m_{i,j})$.

Joint Training with Auxiliary Tasks Patient embedding \mathbf{h} is often used for specific prediction tasks, such as heart failure prediction or mortality. The representation power of \mathbf{h} comes from properly capturing each visit $\mathcal{V}^{(t)}$, and modeling the longitudinal aspect with the function $h(\mathbf{v}_0, \dots, \mathbf{v}_t)$. Since the focus of this work is on modeling a single visit $\mathcal{V}^{(t)}$, we perform auxiliary predictions as follows:

$$\hat{d}_i^{(t)} = p(d_i^{(t)} | \mathbf{o}_i^{(t)}) = \text{softmax}(\mathbf{U}_d \mathbf{o}_i^{(t)}) \quad (4)$$

$$\hat{m}_{i,j}^{(t)} = p(m_{i,j}^{(t)} | \mathbf{o}_i^{(t)}) = \sigma(\mathbf{U}_m \mathbf{o}_i^{(t)}) \quad (5)$$

$$L_{aux} = -\lambda_{aux} \sum_t \left(\sum_i^{|\mathcal{V}^{(t)}|} \left(CE(d_i^{(t)}, \hat{d}_i^{(t)}) + \sum_j^{|\mathcal{M}_i^{(t)}|} CE(m_{i,j}^{(t)}, \hat{m}_{i,j}^{(t)}) \right) \right) \quad (6)$$

Given Dx object embeddings $\mathbf{o}_1^{(t)}, \dots, \mathbf{o}_{|\mathcal{V}^{(t)}|}^{(t)}$, while aggregating them to obtain $\mathbf{v}^{(t)}$ as in Eq. (1), MiME predicts the Dx code $d_i^{(t)}$, and the associated treatment code $m_{i,j}^{(t)}$ as depicted by Figure 2. In Eq. (4) and Eq. (5), $\mathbf{U}_d \in \mathbb{R}^{|\mathcal{A}| \times z}$ and $\mathbf{U}_m \in \mathbb{R}^{|\mathcal{B}| \times z}$ are weight matrices used to compute the prediction of Dx code $\hat{d}_i^{(t)}$ and the prediction of the treatment code $\hat{m}_{i,j}^{(t)}$, respectively. In Eq. (6), T denotes the total number of visits the patient made, $CE(\cdot, \cdot)$ the cross-entropy function and λ_{aux} the coefficient for the auxiliary loss term. We used the softmax function for predicting $d_i^{(t)}$ since in a single Dx object $\mathcal{O}_i^{(t)}$, there is only one Dx code involved. However, there could be no (or many) treatment codes associated with $\mathcal{O}_i^{(t)}$, and therefore we used $|\mathcal{B}|$ number of sigmoid functions for predicting each treatment code.

Auxiliary tasks are based on the inherent structure of the EHR data, and require no additional labeling effort. These auxiliary tasks guide the model to learn Dx object embeddings $\mathbf{o}_i^{(t)}$ that are representative of the specific codes involved with it. Correctly capturing the events within a visit is the basis of all downstream prediction tasks, and these general-purpose auxiliary tasks, combined with the specific target task, encourage the model to learn visit embeddings $\mathbf{v}^{(t)}$ that are not only tuned for the target prediction task, but also grounded in general-purpose foundational knowledge.

3 Experiments

In this section, we first describe the dataset and the baseline models, and present evaluation results. The source code of MiME is publicly available at <https://github.com/mp2893/mime>.

3.1 Source of Data

We conducted all our experiments using EHR data provided by Sutter Health. The dataset was constructed for a study designed to predict a future diagnosis of heart failure, and included EHR data from 30,764 senior patients 50 to 85 years of age. We extracted the diagnosis codes, medication codes and the procedure codes from encounter records, and related orders. We used Clinical Classification Software for ICD9-CM⁴ to group the ICD9 diagnosis codes into 388 categories. Generic Product Identifier Drug Group⁵ was used to group the medication codes into 99 categories. Clinical Classifications Software for Services and Procedures⁶ was used to group the CPT procedure codes into 1,824 categories. Any code that did not fit into the grouper formed its own category. Table 2 summarizes data statistics.

3.2 Baseline Models

First, we use Gated Recurrent Units (GRU) [9] with different embedding strategies to map visit embedding sequence $\mathbf{v}^{(1)}, \dots, \mathbf{v}^{(T)}$ to a patient representation \mathbf{h} :

- **raw**: A single visit $\mathcal{V}^{(t)}$ is represented by a binary vector $\mathbf{x}^{(t)} \in \{0, 1\}^{|\mathcal{A}|+|\mathcal{B}|}$. Only the dimensions corresponding to the codes occurring in that visit is set to 1, and the rest are 0.

⁴<https://www.hcup-us.ahrq.gov/toolssoftware/ccs/ccs.jsp>

⁵<http://www.wolterskluwercdi.com/drug-data/medi-span-electronic-drug-file/>

⁶https://www.hcup-us.ahrq.gov/toolssoftware/ccs_svcsproc/ccssvcproc.jsp

Table 2: Statistics of the dataset

# of patients	30,764
# of visits	616,073
Avg. # of visits per patient	20.0
# of unique codes	2,311 (Dx:388, Rx:99, Proc:1,824)
Avg. # of Dx per visit	1.93 (Max: 29)
Avg. # of Rx per diagnosis	0.31 (Max: 17)
Avg. # of Proc. per diagnosis	0.36 (Max: 10)

- **linear**: The binary vector $\mathbf{x}^{(t)}$ is linearly transformed to a lower-dimensional vector $\mathbf{v}^{(t)} = \mathbf{W}_x \mathbf{x}^{(t)}$ where $\mathbf{W}_x \in \mathbb{R}^{b \times (|\mathcal{A}| + |\mathcal{B}|)}$ is the embedding matrix. This is equivalent to taking the vector representations of the codes (*i.e.* columns of the embedding matrix \mathbf{W}_x) in the visit $\mathcal{V}^{(t)}$, and summing them up to derive a single vector $\mathbf{v}^{(t)} \in \mathbb{R}^b$.
- **sigmoid, tanh, relu**: The binary vector $\mathbf{x}^{(t)}$ is transformed to a lower-dimensional vector $\mathbf{v}^{(t)} = \sigma(\mathbf{W}_x \mathbf{x}^{(t)})$ where we use either *sigmoid*, *tanh*, or *ReLU* for $\sigma(\cdot)$ to add non-linearity to **linear**.
- **sigmoid_{mlp}, tanh_{mlp}, relu_{mlp}**: We add one more layer to **sigmoid**, **tanh** and **relu** to increase their expressivity. The visit embedding is now $\mathbf{v}^{(t)} = \sigma(\mathbf{W}_{x_2} \sigma(\mathbf{W}_{x_1} \mathbf{x}^{(t)}))$ where σ is either sigmoid, tanh or ReLU. We do not test **linear_{mlp}** since two consecutive linear layers can be collapsed to a single linear layer.

Second, we also compare with two advanced embedding methods that are specific designed for modeling EHR data.

- **Med2Vec**: We use Med2Vec [11] to learn visit representations, and use those fixed vectors as input to the prediction model. We test this model as a representative case of unsupervised embedding approach using EHR data.
- **GRAM**: We use GRAM [12], which is equivalent to injecting domain knowledge (ICD9 Dx code tree) to **tanh** via attention mechanism. We test this model as a representative case of incorporating external domain knowledge.

3.3 Prediction Tasks

Heart failure prediction The objective is to predict the first diagnosis of heart failure (HF), given an 18-months observation records discussed in section 3.1. Among 30,764 patients, 3,414 were case patients who were diagnosed with HF within a 1-year window after the 18-months observation. The remaining 27,350 patients were controls. The case-control selection criteria are detailed in [39] and summarized in Appendix B. While an accurate prediction of HF can save a large amount of costs and lives [33], this task is also suitable for assessing how well a model can learn the relationship between the external label (*i.e.* the label information is not inherent in the EHR data) and the features (*i.e.* codes).

We applied logistic regression to the patient representation \mathbf{h} to obtain a value between 0 (no HF onset) and 1 (HF onset). All models were trained end-to-end except **Med2Vec**. We report Area under the Precision-Recall Curve (PR-AUC) in the experiment and Area under the Receiver Operating Characteristic (ROC-AUC) in the appendix, as PR-AUC is considered a better measure for imbalanced data like ours [34, 16]. Implementation and training configurations are described in Appendix C. We also performed *sequential disease prediction (SDP)* (predicting all diagnoses of the next visit at every timestep) where MiME demonstrated superior performance over all baseline models. The detailed description and results of SDP are provided in Appendix H and Appendix I respectively.

3.4 Experiment 1: Varying the Data Size

To evaluate MiME’s performance in another perspective, we created four datasets E_1, E_2, E_3, E_4 from the original data such that each dataset consisted of patients with varying maximum sequence length T_{max} (*i.e.* maximum number of visits). In order to simulate a new hospital collecting patient records over time, we increased T_{max} for each dataset such that 10, 20, 30, 150 for E_1, E_2, E_3, E_4 respectively. Each dataset had 6299 (414 cases), 15794 (1177 cases), 21128 (1848 cases), 27428

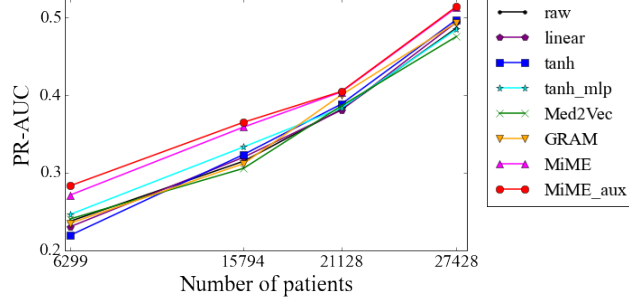


Figure 3: Test PR-AUC of HF prediction for increasing data size. A table with the results of all baseline models is provided in Appendix F

(3173 cases) patients respectively. For MiME_{aux} , we used the same 0.015 for the auxiliary loss coefficient λ_{aux} .

Figure 3 shows the test PR-AUC for HF prediction across all datasets (loss and ROC-AUC are described in Appendix G). Again we show the strongest activation functions **tanh** and **tanh_{mlp}** here and provide the full table in Appendix F. We can readily see that **MiME** outperforms all baseline models across all datasets. However, the performance gap between **MiME** and the baselines are larger in datasets E_1, E_2 than in datasets E_3, E_4 , confirming our assumption that exploiting the inherent structure of EHR can alleviate the data insufficiency problem. Especially for the smallest dataset E_1 , MiME_{aux} (0.2831 PR-AUC) demonstrated significantly better performance than the best baseline **tanh_{mlp}** (0.2462 PR-AUC), showing 15% relative improvement.

It is notable that **MiME** consistently outperformed **GRAM** in both Table 3 and Figure 3 in terms of test loss and test PR-AUC. To be fair, **GRAM** was only using Dx code hierarchy (thus ungrouped 5814 Dx codes were used), and no additional domain knowledge regarding treatment codes. However, the experiment results tell us that even without resorting to external domain knowledge, we can still gain improved predictive performance by carefully studying the EHR data and leveraging its inherent structure.

3.5 Experiment 2: Varying Visit Complexity

Table 3: HF prediction performance on small datasets. Values in the parentheses denote standard deviations from 5-fold random data splits. All models used GRU for mapping the visit embeddings $\mathbf{v}^{(1)}, \dots, \mathbf{v}^{(T)}$ to a patient representation \mathbf{h} . Two best values in each column are marked in bold. A full table with all baselines is provided in Appendix D.

	D₁ (Visit complexity 0-15%) (5608 patients, 464 cases)		D₂ (Visit complexity 15-30%) (5180 patients, 341 cases)		D₃ (Visit complexity 30-100%) (5231 patients, 383 cases)	
	test loss	test PR-AUC	test loss	test PR-AUC	test loss	test PR-AUC
raw	0.2553 (0.0084)	0.2669 (0.0314)	0.2203 (0.0186)	0.2388 (0.0460)	0.2144 (0.0127)	0.3776 (0.0589)
linear	0.2562 (0.0108)	0.2722 (0.0354)	0.2200 (0.0187)	0.2403 (0.0229)	0.2021 (0.0176)	0.4339 (0.0411)
tanh	0.2648 (0.0124)	0.2707 (0.0138)	0.2186 (0.0182)	0.2479 (0.0512)	0.2025 (0.0151)	0.4415 (0.0532)
tanh _{mlp}	0.2587 (0.0121)	0.2671 (0.0257)	0.2289 (0.0213)	0.2296 (0.0185)	0.2024 (0.0181)	0.4290 (0.0510)
Med2Vec	0.2601 (0.0186)	0.2771 (0.0288)	0.2171 (0.0170)	0.2356 (0.0309)	0.2044 (0.0129)	0.3813 (0.0240)
GRAM	0.2554 (0.0254)	0.2633 (0.0521)	0.2249 (0.0448)	0.2505 (0.0609)	0.2333 (0.0362)	0.3998 (0.0628)
MiME	0.2535 (0.0042)	0.2637 (0.0326)	0.2121 (0.0238)	0.2579 (0.0241)	0.1931 (0.0140)	0.4685 (0.0432)
MiME _{aux}	0.2512 (0.0073)	0.2750 (0.0326)	0.2117 (0.0238)	0.2589 (0.0287)	0.1910 (0.0163)	0.4787 (0.0434)

Next, we conducted a series of experiments to confirm that **MiME** can indeed capture the relationship between Dx codes and treatment codes, thus producing robust performance in small datasets. Specifically, we created three small datasets D_1, D_2, D_3 from the original data such that each dataset consisted of patients with varying degree of Dx-treatment interactions (*i.e.* visit complexity). We defined *visit complexity* as below to calculate for a patient the percentage of visits that have at least two diagnosis codes associated with different sets of treatment codes,

$$\text{visit complexity} = \frac{\#\mathcal{V}^{(t)} \text{ where } |\text{set}(\mathcal{M}_1^{(t)}, \dots, \mathcal{M}_{|\mathcal{V}^{(t)}}^{(t)})| \geq 2}{T}$$

where T denotes the total number of visits. For example, in Figure 1, the t -th visit $\mathcal{V}^{(t)}$ has *Fever* associated with no treatments, and *Cough* associated with two treatments. Therefore $\mathcal{V}^{(t)}$ qualifies as a complex visit. From the original dataset, we selected patients with a short sequence (less than 20 visits) to simulate a hospital newly equipped with a EHR system, and there aren't much data collected yet. Among the patients with less than 20 visits, we used visit complexity ranges 0 – 15%, 15 – 30%, 30 – 100% to create D_1, D_2, D_3 consisting of 5608 (464 HF cases), 5180 (341 HF cases), 5231 (383 HF cases) patients respectively. For training MiME with auxiliary tasks, we explored various λ_{aux} values between 0.01 – 0.1, and found 0.015 to provide the best performance, although other values also improved the performance in varying degrees.

Table 3 shows the HF prediction performance for the dataset D_1, D_2 and D_3 . To enhance readability, we show here the results of the strongest activation function **tanh** and **tanh_{mfp}**, and we report test loss and test PR-AUC. The results of other activation functions and the test ROC-AUC are provided in Appendix D and Appendix E.

Table 3 provides two important messages. First of all, both MiME and MiME_{aux} show close to the best performance in all datasets D_1, D_2 and D_3 , especially high complexity dataset D_3 . This confirms that MiME indeed draws its power from the interactions between Dx codes and treatment codes, with or without the auxiliary tasks. In D_1 , patients' visits do not have much structure, that it makes little difference whether we use MiME or not, and its performance is more or less similar to many baselines. Second, auxiliary tasks indeed help MiME generalize better to patients unseen during training. In all datasets D_1, D_2 and D_3 , MiME_{aux} outperforms MiME in all measures, especially in D_3 where it shows PR-AUC 0.4787 (8.4% relative improvement over the best baseline **tanh**).

4 Related Work

Over the years, medical concept embedding has been an active research area. Some works tried to summarize sparse and high-dimensional medical concepts into compressed vectors [15, 18]. In those works, medical concepts were organized as temporal sequences, from which embeddings were derived. Other works used latent layers of deep models for representing more abstract medical concepts [14, 10, 13, 12, 27, 2]. For example, restricted Boltzmann Machines, stacked auto-encoders or multi-layer neural networks were used to learn the representation of codes, visits, or patients [38, 28, 11]. Some works used medical ontologies to learn medical concept representations [12, 8]. Although all works successfully learned concept embeddings for some task in varying degrees, they did not fully utilize the multilevel structure or diagnosis-treatment relationship of EHR.

Recently, multiple code types in EHR gained more attentions. In [35], authors viewed different code types separately, and tried to capture complex relationships across these disparate data types using RNNs, but they did not explicitly address the hierarchy of EHR data. More recently in [30], the authors tried to explicitly capture the interaction between a set of all diagnosis codes and a set of all medication codes occurring in a visit. However, in their experiment, simply concatenating both sets to obtain a visit vector outperformed other methods in many tasks. This suggests that disregarding the diagnosis-specific Dx-Rx interaction and flattening all codes as sets is a suboptimal approach to modeling EHR data.

As described in section 2.2, we employ auxiliary task strategy to train a robust model. Training a model to predict multiple related targets has shown to improve model robustness in medical prediction tasks in previous studies. For example, [5] used lab values as auxiliary targets to improve mortality prediction performance. More recent studies [29, 22, 4] demonstrated improved prediction accuracy when training a model with multiple related tasks such as mortality prediction and phenotyping.

5 Conclusion

In this work, we presented MiME, an integrated approach that simultaneously models hierarchical inter-code relations into medical concept embedding while jointly performing auxiliary prediction tasks. Through extensive empirical evaluation, MiME demonstrated impressive performance across all benchmark tasks and its generalization ability to smaller datasets, especially outperforming baselines in terms of PR-AUC in heart failure prediction. As we have established in this work that MiME can be a good choice for modeling visits, in the future, we plan to extend MiME to include more fine-grained medical events such as procedure outcomes, demographic information, and medication instructions.

Acknowledgments

This work was supported by the National Science Foundation, award IIS-#1418511 and CCF-#1533768, the National Institute of Health award 1R01MD011682-01 and R56HL138415, and Samsung Scholarship. We would also like to thank Sherry Yan for her helpful comments on the original manuscript.

References

- [1] Dzmitry Bahdanau, Kyunghyun Cho, and Yoshua Bengio. Neural machine translation by jointly learning to align and translate. In *ICLR*, 2015.
- [2] Jacek M Bajor and Thomas A Lasko. Predicting medications from diagnostic codes with recurrent neural networks. In *ICLR*, 2017.
- [3] Inci M Baytas, Cao Xiao, Xi Zhang, Fei Wang, Anil K Jain, and Jiayu Zhou. Patient subtyping via time-aware lstm networks. In *SIGKDD*, 2017.
- [4] Adrian Benton, Margaret Mitchell, and Dirk Hovy. Multi-task learning for mental health using social media text. *arXiv preprint arXiv:1712.03538*, 2017.
- [5] Rich Caruana, Shumeet Baluja, and Tom Mitchell. Using the future to "sort out" the present: Rankprop and multitask learning for medical risk evaluation. In *NIPS*, pages 959–965, 1996.
- [6] Chao Che, Cao Xiao, Jian Liang, Bo Jin, Jiayu Zho, and Fei Wang. An rnn architecture with dynamic temporal matching for personalized predictions of parkinson’s disease. In *SIAM on Data Mining*, 2017.
- [7] Zhengping Che, David Kale, Wenzhe Li, Mohammad Taha Bahadori, and Yan Liu. Deep computational phenotyping. In *Proceedings of the 21th ACM SIGKDD International Conference on Knowledge Discovery and Data Mining*, KDD ’15, pages 507–516, New York, NY, USA, 2015. ACM.
- [8] Zhengping Che, David Kale, Wenzhe Li, Mohammad Taha Bahadori, and Yan Liu. Deep computational phenotyping. In *SIGKDD*, 2015.
- [9] Kyunghyun Cho, Bart Van Merriënboer, Caglar Gulcehre, Dzmitry Bahdanau, Fethi Bougares, Holger Schwenk, and Yoshua Bengio. Learning phrase representations using rnn encoder-decoder for statistical machine translation. In *EMNLP*, 2014.
- [10] Edward Choi, Mohammad Taha Bahadori, Andy Schuetz, Walter F Stewart, and Jimeng Sun. Doctor ai: Predicting clinical events via recurrent neural networks. In *MLHC*, 2016.
- [11] Edward Choi, Mohammad Taha Bahadori, Elizabeth Searles, Catherine Coffey, Michael Thompson, James Bost, Javier Tejedor-Sojo, and Jimeng Sun. Multi-layer representation learning for medical concepts. In *SIGKDD*, 2016.
- [12] Edward Choi, Mohammad Taha Bahadori, Le Song, Walter F Stewart, and Jimeng Sun. Gram: Graph-based attention model for healthcare representation learning. In *SIGKDD*, 2017.
- [13] Edward Choi, Mohammad Taha Bahadori, Jimeng Sun, Joshua Kulas, Andy Schuetz, and Walter Stewart. Retain: An interpretable predictive model for healthcare using reverse time attention mechanism. In *NIPS*, 2016.
- [14] Edward Choi, Andy Schuetz, Walter F Stewart, and Jimeng Sun. Using recurrent neural network models for early detection of heart failure onset. *Journal of the American Medical Informatics Association*, 2016.
- [15] Youngduck Choi, Chill Yi-I Chiu, and David Sontag. Learning low-dimensional representations of medical concepts. *AMIA Summits on Translational Science Proceedings*, 2016.
- [16] Jesse Davis and Mark Goadrich. The relationship between precision-recall and roc curves. In *Proceedings of the 23rd international conference on Machine learning*, pages 233–240. ACM, 2006.
- [17] Cristóbal Esteban, Oliver Staeck, Stephan Baier, Yinchong Yang, and Volker Tresp. Predicting clinical events by combining static and dynamic information using recurrent neural networks. In *ICHI*, 2016.

- [18] Wael Farhan, Zhimu Wang, Yingxiang Huang, Shuang Wang, Fei Wang, and Xiaoqian Jiang. A predictive model for medical events based on contextual embedding of temporal sequences. *JMIR medical informatics*, 2016.
- [19] Akira Fukui, Dong Huk Park, Daylen Yang, Anna Rohrbach, Trevor Darrell, and Marcus Rohrbach. Multimodal compact bilinear pooling for visual question answering and visual grounding. In *EMNLP*, 2016.
- [20] Joseph Futoma, Jonathan Morris, and Joseph Lucas. A comparison of models for predicting early hospital readmissions. *JBI*, 2015.
- [21] Yang Gao, Oscar Beijbom, Ning Zhang, and Trevor Darrell. Compact bilinear pooling. In *CVPR*, 2016.
- [22] Hrayr Harutyunyan, Hrant Khachatrian, David C Kale, and Aram Galstyan. Multitask learning and benchmarking with clinical time series data. *arXiv preprint arXiv:1703.07771*, 2017.
- [23] Kaiming He, Xiangyu Zhang, Shaoqing Ren, and Jian Sun. Deep residual learning for image recognition. In *CVPR*, 2016.
- [24] Jin-Hwa Kim, Kyoung-Woon On, Woosang Lim, Jeonghee Kim, Jung-Woo Ha, and Byoung-Tak Zhang. Hadamard product for low-rank bilinear pooling. In *ICLR*, 2017.
- [25] Diederik P Kingma and Jimmy Ba. Adam: A method for stochastic optimization. *arXiv:1412.6980*, 2014.
- [26] Zachary C Lipton, David C Kale, Charles Elkan, and Randall Wetzell. Learning to diagnose with lstm recurrent neural networks. In *ICLR*, 2016.
- [27] Fenglong Ma, Radha Chitta, Jing Zhou, Quanzeng You, Tong Sun, and Jing Gao. Dipole: Diagnosis prediction in healthcare via attention-based bidirectional recurrent neural networks. In *SIGKDD*, 2017.
- [28] Riccardo Miotto, Li Li, Brian A Kidd, and Joel T Dudley. Deep patient: An unsupervised representation to predict the future of patients from the electronic health records. *Scientific reports*, 2016.
- [29] Che Ngufor, Sudhindra Upadhyaya, Dennis Murphree, Daryl Kor, and Jyotishman Pathak. Multi-task learning with selective cross-task transfer for predicting bleeding and other important patient outcomes. In *Data Science and Advanced Analytics (IEEE DSAA)*, pages 1–8, 2015.
- [30] Phuoc Nguyen, Truyen Tran, and Svetha Venkatesh. Rreset: A recurrent model for sequence of sets with applications to electronic medical records. *arXiv:1802.00948*, 2018.
- [31] Nozomi Nori, Hisashi Kashima, Kazuto Yamashita, Hiroshi Ikai, and Yuichi Imanaka. Simultaneous modeling of multiple diseases for mortality prediction in acute hospital care. In *Proceedings of the 21th ACM SIGKDD International Conference on Knowledge Discovery and Data Mining*, KDD '15, pages 855–864, New York, NY, USA, 2015. ACM.
- [32] T. Pham, T. Tran, D. Phung, and S. Venkatesh. Predicting healthcare trajectories from medical records: A deep learning approach. *Journal of Biomedical Informatics*, 2017.
- [33] Veronique L Roger, Susan A Weston, Margaret M Redfield, Jens P Hellermann-Homan, Jill Killian, Barbara P Yawn, and Steven J Jacobsen. Trends in heart failure incidence and survival in a community-based population. *JAMA*, 2004.
- [34] Takaya Saito and Marc Rehmsmeier. The precision-recall plot is more informative than the roc plot when evaluating binary classifiers on imbalanced datasets. *PloS one*, 10(3):e0118432, 2015.
- [35] Harini Suresh, Nathan Hunt, Alistair Johnson, Leo Anthony Celi, Peter Szolovits, and Marzyeh Ghassemi. Clinical intervention prediction and understanding using deep networks. In *MLHC*, 2017.
- [36] Tensorflow Team. Tensorflow: A system for large-scale machine learning. In *OSDI*, 2016.
- [37] JB Tenenbaum and WT Freeman. Separating style and content with bilinear models. *Neural Computation*, 2000.
- [38] Truyen Tran, Tu Dinh Nguyen, Dinh Phung, and Svetha Venkatesh. Learning vector representation of medical objects via emr-driven nonnegative restricted boltzmann machines (enrbm). *Journal of Biomedical Informatics*, 2015.

- [39] Rajakrishnan Vijaykrishnan, Steven R Steinhubl, Kenney Ng, Jimeng Sun, Roy J Byrd, Zahra Daar, Brent A Williams, Shahram Ebadollahi, Walter F Stewart, et al. Prevalence of heart failure signs and symptoms in a large primary care population identified through the use of text and data mining of the electronic health record. *Journal of Cardiac Failure*, 2014.

Table 4: Qualifying ICD-9 codes for heart failure

ICD-9 Code	Description
398.91	Rheumatic heart failure (congestive)
402.01	Malignant hypertensive heart disease with heart failure
402.11	Benign hypertensive heart disease with heart failure
402.91	Unspecified hypertensive heart disease with heart failure
404.01	Hypertensive heart and chronic kidney disease, malignant, with heart failure and with chronic kidney disease stage I through stage IV, or unspecified
404.03	Hypertensive heart and chronic kidney disease, malignant, with heart failure and with chronic kidney disease stage V or end stage renal disease
404.11	Hypertensive heart and chronic kidney disease, benign, with heart failure and with chronic kidney disease stage I through stage IV, or unspecified
404.13	Hypertensive heart and chronic kidney disease, benign, with heart failure and chronic kidney disease stage V or end stage renal disease
404.91	Hypertensive heart and chronic kidney disease, unspecified, with heart failure and with chronic kidney disease stage I through stage IV, or unspecified
404.93	Hypertensive heart and chronic kidney disease, unspecified, with heart failure and chronic kidney disease stage V or end stage renal disease
428.0	Congestive heart failure, unspecified
428.1	Left heart failure
428.20	Systolic heart failure, unspecified
428.21	Acute systolic heart failure
428.22	Chronic systolic heart failure
428.23	Acute on chronic systolic heart failure
428.30	Diastolic heart failure, unspecified
428.31	Acute diastolic heart failure
428.32	Chronic diastolic heart failure
428.33	Acute on chronic diastolic heart failure
428.40	Combined systolic and diastolic heart failure, unspecified
428.41	Acute combined systolic and diastolic heart failure
428.42	Chronic combined systolic and diastolic heart failure
428.43	Acute on chronic combined systolic and diastolic heart failure
428.9	Heart failure, unspecified

A Discussion of Bilinear Pooling

In Eq. (3), $g(d_i, m_{i,j})$ uses a form of bilinear pooling to explicitly capture the interaction between the Dx code and the treatment code. The original bilinear pooling [37] derives a scalar feature f_i between two embeddings \mathbf{x}, \mathbf{y} such that $f_i = \mathbf{x}^T \mathbf{W}_i \mathbf{y}$ where \mathbf{W}_i is a trainable weight matrix. Since we typically extract many features f_0, \dots, f_i , to capture the interaction between two embeddings, bilinear pooling requires us to train multiple weight matrices (*i.e.* weight tensor). Due to this requirement, researchers developed more efficient methods such as compact bilinear pooling [21, 19] and low-rank bilinear pooling [24], which is used in this work.

B Heart Failure Case-Control Selection Criteria

Case patients were 40 to 85 years of age at the time of HF diagnosis. HF diagnosis (HFDx) is defined as: 1) Qualifying ICD-9 codes for HF appeared in the encounter records or medication orders. Qualifying ICD-9 codes are displayed in Table 4. 2) a minimum of three clinical encounters with qualifying ICD-9 codes had to occur within 12 months of each other, where the date of diagnosis was assigned to the earliest of the three dates. If the time span between the first and second appearances of the HF diagnostic code was greater than 12 months, the date of the second encounter was used as the first qualifying encounter. The date at which HF diagnosis was given to the case is denoted as HFDx. Up to ten eligible controls (in terms of sex, age, location) were selected for each case, yielding an overall ratio of 9 controls per case. Each control was also assigned an index date, which is the HFDx of the matched case. Controls are selected such that they did not meet the operational criteria for HF diagnosis prior to the HFDx plus 182 days of their corresponding case. Control subjects were required to have their first office encounter within one year of the matching HF case patient’s first

Table 5: HF prediction performance of all models on small datasets. Values in the parentheses denote standard deviations from 5-fold random data splits. Two best values in each column are marked in bold.

	D_1 (Visit complexity 0-15%, 5608 patients)		D_2 (Visit complexity 15-30%, 5180 patients)		D_3 (Visit complexity 30-100%, 5231 patients)	
	test loss	test PR-AUC	test loss	test PR-AUC	test loss	test PR-AUC
raw	0.2553 (0.0084)	0.2669 (0.0314)	0.2203 (0.0186)	0.2388 (0.0460)	0.2144 (0.0127)	0.3776 (0.0589)
linear	0.2562 (0.0108)	0.2722 (0.0354)	0.2200 (0.0187)	0.2403 (0.0229)	0.2021 (0.0176)	0.4339 (0.0411)
sigmoid	0.2594 (0.0062)	0.2637 (0.0374)	0.2198 (0.0220)	0.2445 (0.0363)	0.2029 (0.0118)	0.4358 (0.0585)
tanh	0.2648 (0.0124)	0.2707 (0.0138)	0.2186 (0.0182)	0.2479 (0.0512)	0.2025 (0.0151)	0.4415 (0.0532)
relu	0.2601 (0.0107)	0.2546 (0.0109)	0.2288 (0.0244)	0.1957 (0.0217)	0.2083 (0.0124)	0.4100 (0.0276)
sigmoid _{mlp}	0.2836 (0.0102)	0.1207 (0.0145)	0.2407 (0.0162)	0.1119 (0.0334)	0.2127 (0.0294)	0.3547 (0.1208)
tanh _{mlp}	0.2587 (0.0121)	0.2671 (0.0257)	0.2289 (0.0213)	0.2296 (0.0185)	0.2024 (0.0181)	0.4290 (0.0510)
relu _{mlp}	0.2650 (0.0088)	0.2463 (0.0148)	0.2288 (0.0235)	0.1982 (0.0298)	0.2144 (0.0202)	0.3872 (0.0476)
Med2Vec	0.2601 (0.0186)	0.2771 (0.0288)	0.2171 (0.0170)	0.2356 (0.0309)	0.2044 (0.0129)	0.3813 (0.0240)
GRAM	0.2554 (0.0254)	0.2633 (0.0521)	0.2249 (0.0448)	0.2505 (0.0609)	0.2333 (0.0362)	0.3998 (0.0628)
MiME	0.2535 (0.0042)	0.2637 (0.0326)	0.2121 (0.0238)	0.2579 (0.0241)	0.1931 (0.0140)	0.4685 (0.0432)
MiME _{aux}	0.2512 (0.0073)	0.2750 (0.0326)	0.2117 (0.0238)	0.2589 (0.0287)	0.1910 (0.0163)	0.4787 (0.0434)

office visit, and have at least one office encounter 30 days before or any time after the case’s HF diagnosis date to ensure similar duration of observations among cases and controls.

C Training Details

All models were implemented in TensorFlow 1.4 [36], and trained with a system equipped with Intel Xeon E5-2620, 512TB memories and 8 Nvidia Pascal Titan X’s. We used Adam [25] for optimization, with the learning rate $1e - 3$.

In all experiments, the reported results are averaged over 5-fold random data splits: training (70%), validation (10%) and test (20%). All models were trained with the minibatch of 20 patients for 20,000 iterations to guarantee convergence. At every 100 iterations, we evaluated the loss value of the validation set for early stopping.

For the non-linear activation functions in MiME, we used ReLU in all places except for the one in Eq. (1) where we used sigmoid to benefit from its regularization effect. We avoid the vanishing gradient problem by using the skip connections. Note that simply adding skip connections to **sigmoid_{mlp}** did not improve performance.

For the first experiment in section 3.5, size of the visit vector \mathbf{v} was 128 in all baseline models except **raw**. We ran a number of preliminary experiments with values 64, 128, 256 and 512, and we concluded that 128 was sufficient for all models to obtain optimal performance, as the datasets D_1, D_2 and D_3 were rather small. For MiME, we adjusted the size of the embeddings z to match the number of parameters to the baselines. **Med2Vec** was also trained to obtain 128 dimensional visit vectors. Note that **sigmoid_{mlp}**, **tanh_{mlp}**, **relu_{mlp}** and **GRAM** used 128×128 more parameters than other models. We used L_2 regularization with the coefficient $1e - 4$ for all models. We did not use any dropout technique. All models used GRU for the function $h(\mathbf{v}^{(1)}, \dots, \mathbf{v}^{(T)})$ as described in section 3.3, the cell size of which was 128.

For the second experiment in section 3.4, where the models were trained on gradually larger datasets E_1, E_2, E_3 and E_4 , the size of \mathbf{v} was set to 256 for all baseline models except **raw**. The same adjustments were made to MiME as before, and the cell size of GRU was also set to 256.

D Heart Failure Prediction Performance on Datasets D_1, D_2 and D_3 , Full Version

Table 5 shows the performance of all models on datasets D_1, D_2 and D_3 . An interesting finding is that both **sigmoid** and **tanh** mostly outperform **relu** in both measures in D_1, D_2 and D_3 , although *ReLU* is the preferred nonlinear activation for hidden layers in many studies. This seems due to the regularizing effect of *sigmoid* and *tanh* functions. Whereas *ReLU* can produce outputs as high as infinity, *sigmoid* and *tanh* have bounded outputs. Considering that **sigmoid**, **tanh** and **relu** all sum up the code embeddings in a visit $\mathcal{V}^{(t)}$ before applying the nonlinear activation, constraining the output of the nonlinear activation seems to work favorably, especially in D_3 where there are more

codes per visit. This regularization benefit, however, diminishes as the dataset grows, which can be confirmed by Table 7 in section F. In addition, as can be seen by the performance of **sigmoid**_{mlp}, *sigmoid* clearly suffers from the vanishing gradient problem as opposed to *tanh* or *ReLU* that have larger gradient values.

E ROC-AUC of Heart Failure Prediction on Datasets D_1 , D_2 and D_3

Table 6: ROC-AUC of all models for HF prediction on small datasets. Values in the parentheses denote standard deviations from 5-fold random data splits. Two best values in each column are marked in bold.

	D₁ (Visit complexity 0-15%, 5608 patients)	D₂ (Visit complexity 15-30%, 5180 patients)	D₃ (Visit complexity 30-100%, 5231 patients)
raw	0.7424 (0.0153)	0.7508 (0.0254)	0.8130 (0.0315)
linear	0.7298 (0.0187)	0.7241 (0.0220)	0.8209 (0.0130)
sigmoid	0.7220 (0.0098)	0.7331 (0.0475)	0.8280 (0.0128)
tanh	0.7273 (0.0050)	0.7244 (0.0175)	0.8171 (0.0151)
relu	0.7326 (0.0133)	0.7078 (0.0181)	0.8166 (0.0211)
sigmoid _{mlp}	0.5520 (0.0136)	0.5770 (0.0416)	0.7718 (0.0826)
tanh _{mlp}	0.7215 (0.0188)	0.7058 (0.0261)	0.8080 (0.0258)
relu _{mlp}	0.7205 (0.0122)	0.7014 (0.0177)	0.7993 (0.0212)
Med2Vec	0.7447 (0.0194)	0.7515 (0.0243)	0.8325 (0.0254)
GRAM	0.7586 (0.0240)	0.6930 (0.0379)	0.7785 (0.0260)
MiME	0.7433 (0.0127)	0.7723 (0.0232)	0.8393 (0.0281)
MiME _{aux}	0.7449 (0.0117)	0.7741 (0.0209)	0.8437 (0.0244)

Table 6 shows ROC-AUC of all models on datasets D_1 , D_2 and D_3 . Except for D_1 where patients have low visit complexity, MiME again consistently outperforms all baseline models. However, the ROC-AUC gap between MiME and baselines is not as great as PR-AUC. This is because ROC-AUC is determined by sensitivity (*i.e.* recall, or true positive rate) and specificity (*i.e.* true negative rate). A model achieves a high specificity if it can correctly identify as many negative samples as possible, which is easier for problems with many negative samples and few positive samples. PR-AUC, on the other hand, is determined by precision and recall. Therefore, for a model to achieve a high PR-AUC, it must correctly retrieve as many positive samples as possible while ignoring negative samples, which is harder for problems with few positive samples.

For heart failure (HF) prediction, achieving high specificity is relatively easy as there are way more controls (*i.e.* negative samples) than cases (*i.e.* positive samples). However, correctly identifying cases while ignoring controls requires a model to recognize what differentiates cases from controls. This means paying attention to the details of the patient records, such as the relationship between the diagnosis codes and treatment codes. That is why MiME shows significant improvement in PR-AUC while showing moderate improvement in ROC-AUC. Also, this also explains why **Med2Vec** shows very poor PR-AUC as opposed to its competitive ROC-AUC. Med2Vec only pays attention to the co-occurrence of codes within a single visit, and not the interaction between diagnosis codes and treatment codes. It can work as a very efficient code grouper (codes that often appear in the same visit end up having similar code embeddings), leading to a increased ROC-AUC. But it cannot achieve a high PR-AUC, as that code grouping loses much of the subtle interaction between diagnosis codes and medication codes.

F Test PR-AUC on Datasets E_1 , E_2 , E_3 and E_4 , Full Version

Table 7 shows the PR-AUC of all models on datasets E_1 , E_2 , E_3 and E_4 . It is notable that some baseline models show fluctuating performance as dataset grows. For example, **tanh**_{mlp} showed competitive performance in small datasets, but weaker performance in large datasets. **relu**_{mlp}, on the other hand, did not stand out in small datasets, but became the best baseline in large datasets. Such behaviors, along with the finding in Appendix D regarding the regularization effect, suggest that we should carefully choose activation functions of our model depending on the dataset size.

G Test Loss and Test ROC-AUC on Datasets E_1 , E_2 , E_3 and E_4

Table 8 and Table 9 respectively shows the test loss and test ROC-AUC of all models on datasets of varying sizes E_1 , E_2 , E_3 and E_4 . Both MiME and MiME_{aux} consistently outperformed all baselines

Table 7: Test PR-AUC of HF prediction for increasing data size. Parentheses denote standard deviations from 5-fold random data splits. The two strongest values in each column are marked bold.

	E₁ (6299 patients)	E₂ (15794 patients)	E₃ (21128 patients)	E₄ (27428 patients)
raw	0.2374 (0.0514)	0.3149 (0.0367)	0.3816 (0.0290)	0.4865 (0.0219)
linear	0.2303 (0.0467)	0.3200 (0.0353)	0.3806 (0.0271)	0.4939 (0.0159)
sigmoid	0.2354 (0.0355)	0.3260 (0.0392)	0.3851 (0.0235)	0.4823 (0.0195)
tanh	0.2192 (0.0407)	0.3235 (0.0441)	0.3884 (0.0310)	0.4973 (0.0262)
relu	0.2293 (0.0459)	0.3274 (0.0359)	0.3793 (0.0291)	0.4957 (0.0160)
sigmoid _{mlp}	0.0843 (0.0154)	0.0919 (0.0110)	0.1333 (0.0047)	0.2221 (0.0146)
tanh _{mlp}	0.2462 (0.0675)	0.3333 (0.0387)	0.3834 (0.0209)	0.4847 (0.0172)
relu _{mlp}	0.2353 (0.0335)	0.3111 (0.0494)	0.3976 (0.0235)	0.4983 (0.0229)
Med2Vec	0.2404 (0.0228)	0.3057 (0.0508)	0.3861 (0.0343)	0.4756 (0.0148)
GRAM	0.2349 (0.0424)	0.3118 (0.0337)	0.4002 (0.0113)	0.4936 (0.0199)
MiME	0.2711 (0.0308)	0.3589 (0.0533)	0.4041 (0.0231)	0.5129 (0.0204)
MiME _{aux}	0.2831 (0.0425)	0.3651 (0.0473)	0.4047 (0.0276)	0.5142 (0.0210)

in terms of both test loss and test ROC-AUC, except **Med2Vec**. Moreover, MiME_{aux} always showed better performance than MiME except test loss in E_4 , especially for the smallest dataset E_1 , confirming our assumption that auxiliary tasks can train a robust model when large datasets are unavailable. **tanh_{mlp}** consistently showed good performance in terms of ROC-AUC across all datasets, as opposed to showing fluctuating PR-AUC in Table 7. **Med2Vec** again showed a competitive ROC-AUC in all datasets, even outperforming MiME_{aux} in E_3 . This suggests that initializing MiME’s code embeddings with Med2Vec can be an interesting future direction as it may lead to an even better performance.

Table 8: Test loss of HF prediction for increasing data size. Parentheses denote standard deviations from 5-fold random data splits. Two best values in each column are marked bold.

	E₁ (6299 patients)	E₂ (15794 patients)	E₃ (21128 patients)	E₄ (27428 patients)
raw	0.2204 (0.0090)	0.2236 (0.0166)	0.2387 (0.0045)	0.2658 (0.0095)
linear	0.2229 (0.0078)	0.2245 (0.0160)	0.2395 (0.0068)	0.2642 (0.0099)
sigmoid	0.2229 (0.0064)	0.2215 (0.0135)	0.2373 (0.0034)	0.2655 (0.0095)
tanh	0.2232 (0.0082)	0.2217 (0.0142)	0.2396 (0.0068)	0.2629 (0.0098)
relu	0.2253 (0.0058)	0.2236 (0.0134)	0.2436 (0.0104)	0.2637 (0.0104)
sigmoid _{mlp}	0.2487 (0.0109)	0.2681 (0.0140)	0.2964 (0.0054)	0.3335 (0.0063)
tanh _{mlp}	0.2198 (0.0058)	0.2259 (0.0156)	0.2358 (0.0024)	0.2616 (0.0111)
relu _{mlp}	0.2175 (0.0067)	0.2263 (0.0144)	0.2402 (0.0037)	0.2668 (0.0090)
Med2Vec	0.2162 (0.0091)	0.2141 (0.0171)	0.2340 (0.0043)	0.2631 (0.0106)
GRAM	0.2321 (0.0118)	0.2291 (0.0154)	0.2382 (0.0036)	0.2663 (0.0071)
MiME	0.2128 (0.0075)	0.2153 (0.0126)	0.2331 (0.0039)	0.2559 (0.0096)
MiME _{aux}	0.2111 (0.0089)	0.2122 (0.0115)	0.2326 (0.0048)	0.2557 (0.0095)

Table 9: Test ROC-AUC of HF prediction for increasing data size. Parentheses denote standard deviations from 5-fold random data splits. Two best values in each column are marked bold.

	E₁ (6299 patients)	E₂ (15794 patients)	E₃ (21128 patients)	E₄ (27428 patients)
raw	0.7585 (0.0202)	0.8003 (0.0265)	0.8165 (0.0146)	0.8330 (0.0111)
linear	0.7411 (0.0252)	0.7945 (0.0181)	0.8129 (0.0140)	0.8377 (0.0119)
sigmoid	0.7236 (0.0286)	0.7978 (0.0163)	0.8154 (0.0167)	0.8343 (0.0121)
tanh	0.7419 (0.0247)	0.7943 (0.0186)	0.8121 (0.0146)	0.8388 (0.0117)
relu	0.7366 (0.0267)	0.7891 (0.0197)	0.8105 (0.0210)	0.8353 (0.0123)
sigmoid _{mlp}	0.5191 (0.0269)	0.5356 (0.0365)	0.6013 (0.0082)	0.6628 (0.0176)
tanh _{mlp}	0.7429 (0.0330)	0.7796 (0.0283)	0.8172 (0.0084)	0.8431 (0.0128)
relu _{mlp}	0.7496 (0.0425)	0.7837 (0.0217)	0.8047 (0.0131)	0.8331 (0.0100)
Med2Vec	0.7633 (0.0151)	0.8141 (0.0213)	0.8301 (0.0138)	0.8445 (0.0115)
GRAM	0.7575 (0.0218)	0.7828 (0.0228)	0.8077 (0.0107)	0.8313 (0.0083)
MiME	0.7676 (0.0292)	0.8109 (0.0223)	0.8267 (0.0106)	0.8471 (0.0100)
MiME _{aux}	0.7824 (0.0213)	0.8154 (0.0193)	0.8281 (0.0159)	0.8478 (0.0108)

H Sequential Disease Prediction

Sequential disease prediction In order to test if leveraging EHR’s inherent structure is a strategy generalizable beyond heart failure prediction, we test MiME’s prediction performance in another context, namely sequential disease prediction. The objective is to predict the diagnosis codes occurring in visit $\mathcal{V}^{(t+1)}$, given all past visits $\mathcal{V}^{(1)}, \mathcal{V}^{(2)}, \dots, \mathcal{V}^{(t)}$. The input features are diagnosis codes \mathcal{A} and treatment codes \mathcal{B} , while the output space only consists of diagnosis codes \mathcal{A} . This task is useful for preemptively assessing the patient’s potential future risk [10], but is also appropriate for assessing how well a model captures the progression of the patient status over time. We used GRU as the mapping function $h(\cdot)$, and hidden vectors from all timesteps were fed to the softmax function with $|\mathcal{A}|$ output classes to perform sequential prediction.

I Experiment Results for Sequential Disease Prediction

Table 10: Prediction performance for sequential disease prediction. Values in the parentheses denote standard deviations from 5-fold random data splits. The best value in each column is marked in bold.

	Test loss	Test recall@5	Test recall@10	Test recall@20
raw	7.2121 (0.0319)	0.5329 (0.0016)	0.6600 (0.0016)	0.7749 (0.0019)
linear	7.1474 (0.0321)	0.5443 (0.0008)	0.6749 (0.0010)	0.7876 (0.0009)
sigmoid	7.3494 (0.0438)	0.5110 (0.0054)	0.6338 (0.0052)	0.7529 (0.0029)
tanh	7.1439 (0.0313)	0.5456 (0.0016)	0.6755 (0.0012)	0.7879 (0.0010)
relu	7.1576 (0.0285)	0.5427 (0.0011)	0.6716 (0.0016)	0.7846 (0.0015)
sigmoid _{mlp}	8.7886 (0.0257)	0.2132 (0.0038)	0.3466 (0.0031)	0.5158 (0.0044)
tanh _{mlp}	7.1392 (0.0302)	0.5470 (0.0010)	0.6788 (0.0006)	0.7926 (0.0009)
relu _{mlp}	7.1719 (0.0334)	0.5433 (0.0010)	0.6744 (0.0010)	0.7876 (0.0012)
Med2Vec	7.2429 (0.0283)	0.5317 (0.0011)	0.6583 (0.0020)	0.7752 (0.0016)
GRAM	7.1738 (0.0361)	0.5390 (0.0016)	0.6685 (0.0025)	0.7830 (0.0015)
MiME	7.1224 (0.0326)	0.5496 (0.0010)	0.6815 (0.0009)	0.7945 (0.0014)

After training all models until convergence, performance was measured by sorting the predicted diagnosis codes for $\mathcal{V}^{(t+1)}$ by their prediction values, and calculating *Recall@k* using the true diagnosis codes of $\mathcal{V}^{(t+1)}$.

Table 10 shows the performance of all models for sequential disease prediction. MiME demonstrated the best performance in all metrics, showing that MiME can properly capture the temporal progression of the patient status. It is noteworthy that **linear** displayed very competitive performance compared to the best performing models. This is due to the fact that chronic conditions such as hypertension or diabetes persist over a long period of time, and sequentially predicting them becomes an easy task that does not require an expressive model. This was also reported in [10] where a strategy to choose the most frequent diagnosis code as the prediction showed competitive performance in a similar task.

In order to study whether explicitly incorporating the structure of EHR helps when there are small data volume, we calculated the test performance in terms of *Precision@5* for predicting each diagnosis (Dx) code of \mathcal{A} . In Table 11, we report average *Precision@5* for four different groups of Dx codes, where the groups were formed by the rarity/frequency of the Dx codes in the training data. For example, the first column represents the Dx codes that appear in the 0.01%-0.05% of the entire visits (433407) in the training data, which are very rare diseases. On the other hand, the Dx codes in the last column appear in maximum 13.39% of the visits, indicating high-prevalence diseases. We selected the best performing activation function **tanh** among the three.

As can be seen from Table 11, except for the rarest Dx codes, MiME outperforms all other baseline models, as much as 11.6% relative gain over **tanh_{mlp}**. It is notable that **Med2Vec** demonstrated the greatest performance for the rarest Dx code group. However, the benefit of using pre-trained embedding vectors quickly diminishes to the point of degrading the performance when there are at least several hundred training samples.

Overall, MiME demonstrated good performance in prediction tasks in diverse settings, and it is notable that they significantly outperformed the baseline models in the more complex task, namely HF

Table 11: Accuracy@5 for predicting diseases grouped by their rarity. The prevalence percentages are calculated by dividing the number of occurrences of each disease by 433407, the total number of visits in the training data. All values are averaged from 5-fold cross validation.

Model	20th-40th percentile (0.01%-0.05% preval)	40th-60th percentile (0.05%-0.2% preval)	60th-80th percentile (0.2%-0.8% preval)	80th-100th percentile (0.8%-13.4% preval)
raw	0.0530 (0.0156)	0.1907 (0.0128)	0.2999 (0.0039)	0.4304 (0.0052)
linear	0.0633 (0.0203)	0.2162 (0.0163)	0.3266 (0.0053)	0.4388 (0.0051)
tanh	0.0674 (0.0182)	0.2101 (0.0143)	0.3218 (0.0045)	0.4379 (0.0033)
tanh _{mlp}	0.0723 (0.0165)	0.2353 (0.0118)	0.3388 (0.0044)	0.4381 (0.0034)
Med2Vec	0.1156 (0.0101)	0.2240 (0.0155)	0.3177 (0.0076)	0.4217 (0.0046)
GRAM	0.0574 (0.0121)	0.1634 (0.0057)	0.3053 (0.0089)	0.4409 (0.0039)
MiME	0.0965 (0.0154)	0.2625 (0.0209)	0.3597 (0.0082)	0.4447 (0.0034)

prediction, where the relationship between the label and the features (*i.e.* codes) from the data was more than straightforward.